euspen's 23rd International Conference & Exhibition, Copenhagen, DK, June 2023
www.euspen.eu

Measurement of additively manufactured lattice struts: an analysis of defect basis representation performance with virtual volume correlation

Marc-Antoine de Pastre[1], Yann Quinsat[1]

[1]LURPA, ENS Paris-Saclay, Université Paris-Saclay, 91190 Gif-sur-Yvette, France

marc-antoine.de_pastre@ens-paris-saclay.fr

Abstract
Additive manufacturing (AM) considerably widens design freedom and allows the manufacturing of complex geometries. These complex geometries, such as lattice structures, are not free from defects. Metrologists and manufacturers then work together to measure, understand, and correct defects introduced during AM. Metrologists in particular use X-ray computed tomography (XCT) to reveal both external and internal defects that would not be accessible to traditional optical measurements. Whereas existing methods to extract geometry from volumetric XCT measurement mainly rely on thresholding, other recently developed methods circumvent the need to choose thresholding values. The virtual volume correlation (V2C) method, for example, involves neither thresholding nor user-dependent step to directly extract geometrical and dimensional defects from lattice structure volumetric data. However, V2C requires a defined defect basis in order to decompose the measured defect into a sum of elementary defects. This paper investigates three different defect bases: analytical, strut natural 3D vibrations, and Laplace-Beltrami eigenfunctions. Each of these bases are implemented with V2C to represent metal powder bed fusion (PBF) lattice strut geometrical and dimensional defects. The basis suitability to represent the defect is estimated, and the representation efficiencies are compared. The paper concludes by analysing which of the three bases are the most representative and the most adapted to the V2C methodology with a reliable computation time.

Computed tomography, lattice strut, virtual volume correlation, defect representation

1. Introduction

Additive manufacturing (AM) enables the production of complex geometries that cannot be achieved by traditional manufacturing processes [1]. Lattice structures, which consist of the 3D repetition of an unit cell, illustrate this complexity. Optical measurement of these structures is then challenging as features of interest may be internal to the matter, or hidden by the surrounding features [2].

By its volumetric nature, X-ray computed tomography (XCT) is an efficient tool to reveal features that are not accessible to optical measurement [3]. XCT measurement is a three-fold procedure: projection, reconstruction, and surface determination. Whereas projection and reconstruction are mainly performed by reliable and systematic algorithms, surface determination is more debated. From the reconstructed volume, surface determination consists in sorting grey-level voxels composing the volume to identify the measured material boundary. Above the existing surface determination methodologies, such as global or local-adaptive thresholding, the literature shows there is no standard procedure. Surface determination methodology remains the user's choice. However, discrepancies have been observed between the thresholding methodologies [4].

The virtual volume correlation (V2C) methodology has recently been proposed [5, 6] as an alternative surface determination procedure for identifying geometrical and dimensional defects. Relying on a defined defect basis, a virtual volume with known geometry is successively deformed until the difference with the XCT reconstructed volume is minimised. That methodology does not require surface determination. With V2C, the defect representation suitability is deeply linked to the chosen defect basis. Defect basis is the collection of deformation modes whose sum best fits the measured defect. Previous work [5] relied on an analytical basis proposed in the tolerance analysis field [7] for implementation simplicity on cylinder shape. However, this work showed the limitation of this defect basis. This basis neither represent non-regular defects nor integrate surface quality defects where lower wavelength defects stay out of the scope of study.

In order to better represent these lower wavelength defects, other defect bases are considered as alternative defect descriptors. This paper investigates the effect of the chosen defect basis on the defect representation for AM lattice struts.

This paper is organised as follows. Section **2** details each of the considered defect basis as well as the undertaken methodology. Section **3** presents the analysis context where comparative results are extracted between the computed correlated geometries and computer-aided design (CAD) and $ISO_{50\%}$ geometries. These results are discussed in Section **4** where bases are compared by observed deviations and computation requirements.

2. Methodology and defect bases

2.1. V2C overview

V2C consists in identifying the displacement field $\mathbf{u}$ embedded in the physical volume f, by iteratively deforming the virtual volume g. The correlation score Φ over the region of interest (ROI) of the measured volume is defined in equation **1**:

$$\Phi(\mathbf{u}) = \iiint_{ROI} [f(\mathbf{X}) - g(\mathbf{X} + \mathbf{u})]^2 \, d\Omega \tag{1}$$

The displacement field $\mathbf{u}$ is assumed to be expressed by modal decomposition as detailed in equation **2** :

$$\mathbf{u} = \sum_k \lambda_k \mathbf{u}_k \tag{2}$$

where $\mathbf{u}_k$ are the elementary modes which expression are known. The collection $\{\boldsymbol{u}_k\}_{k=\{1,\ldots,N\}}$ composes the defect basis. λ_k is the modal amplitude (also referred as modal participation in the literature) that should be identified by minimising the correlation score Φ:

$$\{\boldsymbol{\lambda}_{\boldsymbol{min}}\} = \underset{\boldsymbol{\lambda}}{argmin}\, \Phi\,(\boldsymbol{u}) \tag{3}$$

In the following, three defect bases $\{\boldsymbol{u}_k\}_{k=\{1,\ldots,N\}}$ are considered for identifying AM lattice strut geometrical and dimensionnal defects. The considered modes will then be adapted to strut geometry.

2.2. Defect bases

2.2.1. Analytical basis

The analytical defect basis is composed of the overall defect decomposition into simpler defects. The decomposition for cylindrical struts is three-fold: registration modes, vertical modes, and plane modes. Registration mode corrects the virtual geometry towards its position or radius dilatation deviation. Vertical modes such as hourglass of vertical waviness consider the geometry variability along the strut axis. Plane modes illustrate the effect of similar defects all along the strut axis and are defined in a strut plane. Figure **1** depicts the decomposition. This paper considers the following analytical modes: rigid registration, dilatation, taper, hourglass, 2 waviness modes along the strut axis, and 20 plane modes. This configuration was chosen according to previous work [5].

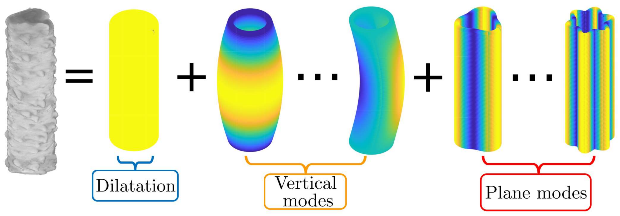

Figure 1: Analytical modes representation

2.2.2. 3D Vibration basis

The 3D vibration basis [8] is generated from the CAD model using the CATIA Generative Structural Analysis workbench. In this workbench, a free frequency analysis is performed from the meshed strut and vibration displacement fields are generated for the first 300 natural vibrating modes. Figure **2** illustrates some of the developed modes.

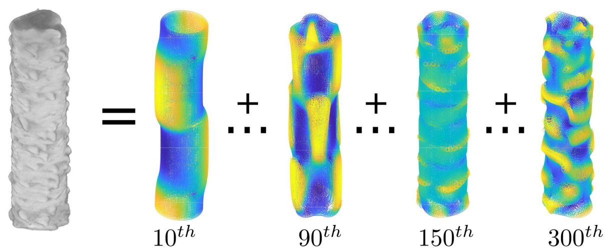

Figure 2: 3D vibration modes representation

2.2.3. Laplace-Beltrami eigenfunctions basis

Laplace-Beltrami (LB) operator is the generalisation of the Laplacian operator to Riemann manifolds. The discretisation of the LB operator over a mesh is explained in [9], where meshed surface is described by a discrete signal. According to Fourier transform theory, eigenvectors' decomposition of this signal leads to elementary displacement eigenfunctions. The sum of these eigenfunctions, weighted by eigenvalues, reconstructs the original signal. In this paper, displacement fields are generated for the first 300 LB modes. Figure **3** shows the LB decomposition from the $ISO_{50\%}$ surface mesh.

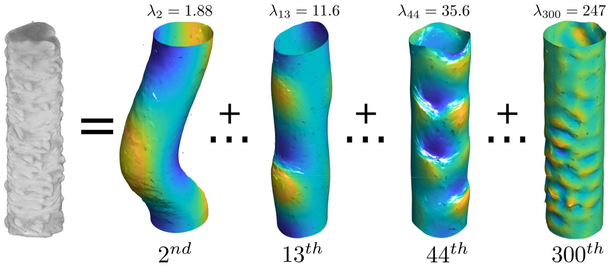

Figure 3: LB modes representation

3. Analysis context

Each of the previously defined bases is successively implemented in the V2C code where the sample and the analysis context is described in the following section.

3.1. Sample manufacturing and measurement

The sample is a vertical strut representative of an AM lattice structure. The strut has a 0.6 mm radius and a 5 mm length, designed in a CAD software. The lattice structure was produced by laser powder bed fusion (LPBF) on an Addup FormUp 350 using Inconel 718 powder and the printing parameters displayed in Table **1**.

Table 1: Printing parameters

Powder	Inconel 718
Layer thickness	40 µm
Laser power	220 W
Scan speed	2100 mm.s^{-1}
Contour scan power	210 W
Contour scan speed	1800 mm.s^{-1}
Hatch space	55 µm

The manufactured sample was washed with water and dried with compressed air. It was removed from the substrate using an electrical discharge machine. To avoid any edge effect resulting from the substrate removal, the region of study was reduced to a 4 mm length.

The sample was then measured using XCT and the following parameters. Instrument: North Star Imaging X50, X-rays source: XRayWorX, Detector: Dexela 292, geometric magnification of 33 leading to a voxel size of 4.5 µm, tube voltage 150 kV, tube current 40 µA. A warmup scan of approximately 30 minutes was performed prior to the scan. Volumetric reconstruction was performed from 900 projections in the manufacturer's software, using a filtered backprojection algorithm and a beam hardening correction without specific filter. Projections were saved in a .raw file format.

3.2. Analysis workflow

V2C is applied to the reconstructed data relying successively on the three defect bases. V2C then outputs three geometries deformed relative to their defect basis. Cloud-to-mesh distances are separately computed between these deformed geometries,

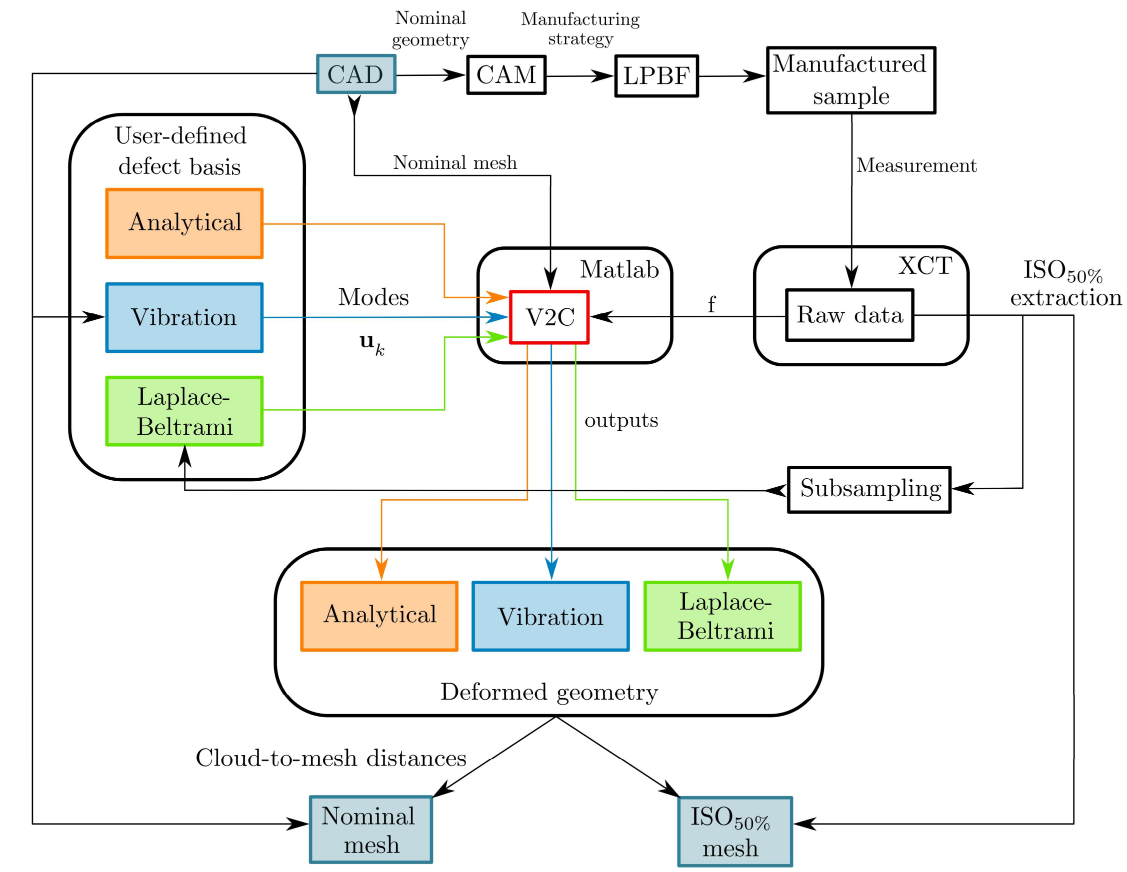

Figure 4: Data processing pipeline

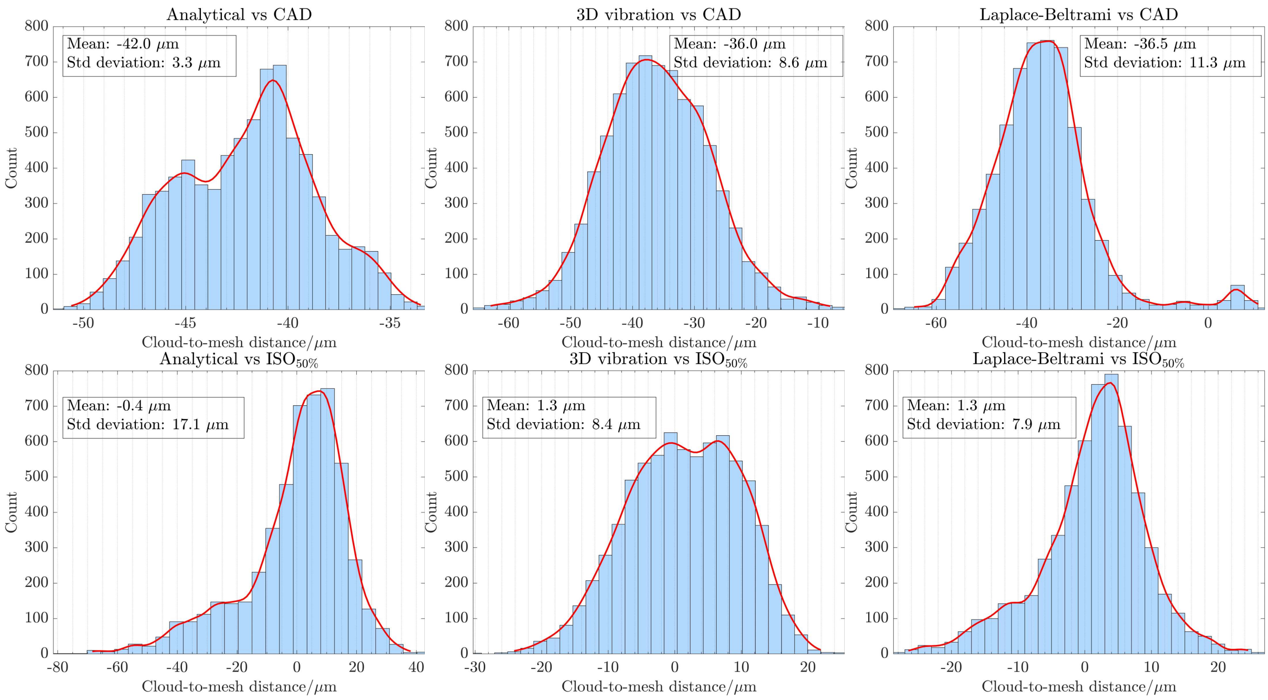

Figure 5: Cloud-to-mesh distances between correlated and CAD geometries (top); between correlated and ISO$_{50\%}$ geometries (bottom)

and both nominal mesh extracted from the CAD model and the ISO$_{50\%}$ mesh determined from the XCT reconstructed volume. Figure **4** summarises the undertaken data pipeline.

3.3. Results

Figure **5** shows the cloud-to-mesh deviation distributions between each of the correlated geometries and the meshed CAD model as well as the meshed surface-determined ISO$_{50\%}$. In these histograms, the bin number was chosen according to the Sturges rule.

Comparison datapoints were further raster-scanned to meet the density of the least dense dataset. Such representations allow two interpretation fields: the efficiency of one basis compared to another, and the degree of similarity of correlated geometries.

Table **2** shows the computing parameters required for generating correlated geometries. All computations were performed using Matlab on a high-performance computing (HPC) cluster.

Table 2: Computation requirements according to the defect basis

Defect basis	Real Time	Needed RAM/Gb
Analytical	2h36mins	392
3D Vibration	18h56mins	112
LB	20h28mins	221

4. Discussion

As shown in Figure **5**, when correlated geometries are compared to the meshed CAD model, each comparison dataset indicates a negative mean value. This result illustrates the contraction effect of the strut whilst manufacturing with the LPBF process. In addition, the standard deviation values of each correlated geometry compared to the meshed CAD model show how V2C identifies defects embedded in the physical volume: the vibrational and LB bases have increased standard deviation values for the CAD comparison. In this case, the vibrational basis and the LB basis include surface quality defects in their representation because, as a first approach, the cut-off number of modes was arbitrarily set. Consequently, lower wavelength defects belonging to surface quality defects are not optimally taken into account. However, the cloud-to-mesh distances range is narrower for the analytical basis than the vibration or the LB bases.

The $ISO_{50\%}$ mesh is closer to the real manufactured part geometry than the CAD mesh. The mean values are centred when correlated geometries are compared to the $ISO_{50\%}$ mesh. The analytical defect basis dataset compared to the $ISO_{50\%}$ mesh even shows a quasi-null mean value. With the adopted configuration of the analytical defect basis, overall surface defects are smoothed and averaged, leading to this mean-centred value for all correlated geometries. Their reduced standard deviation values show the advantage of both vibrational and LB bases in comparison to the analytical defect basis. The former bases integrate surface quality defects in the identification process that is not permitted by the analytical defect basis. The voxel size of 9 microns should also be reminded as a limit of further interpretation of the obtained standard deviation results.

Arguments for considering a defect basis rather than another would also rely on the computation performances, as shown in Table **2**. Analytical basis requires less computation time but a large amount of RAM to provide only with geometrical and dimensional defects. The basis has few defined modes and a dense deformed mesh. On the contrary, the vibrational and the LB bases require less RAM but an increased computation time to provide with geometrical and dimensional defects as well as lower wavelength defects. These bases have more defined modes and reduced deformed mesh densities. These discrepancies are explained by the generation of the defect bases and the datapoints being handled. Whereas analytical basis point density can be directly set in the V2C code, vibrational basis depends on the CAD mesh density and the vibrational modes generated on Catia. LB eigenfunctions are generated from the $ISO_{50\%}$ mesh i.e., a very dense mesh. The latter requires a sampling step (see Figure **4**) to compute the LB modes in a reasonable time.

5. Conclusion

This work investigates three defect bases to identify LPBF geometrical and dimensional defects relying on the V2C methodology. These defect bases are the analytical basis defined inside the V2C code, the 3D vibrational basis generated from CATIA modal analysis, and the LB eigenfunctions basis computed from the strut $ISO_{50\%}$ mesh. Whereas the analytical basis is limited to geometrical and dimensional defects, vibrational and LB bases represent lower wavelength defects. Each of these bases requires different numerical resources due to the diverse nature of basis generation. Whereas the analytical basis was generated within V2C, the LB eigenfunctions require subsampling of the $ISO_{50\%}$ mesh. These preparation steps alter the computation requirements.

For each of these bases, the number of modes to take into account should be linked to the desired defect representativity. This paper only aims at providing a proof of concept study, and the number of modes for vibrational and LB bases was arbitrarily set; further work regarding the defect representativity should be undertaken. This complementary study, already performed for the analytical defect basis, would be the object of future work for both vibrational and LB bases.

Acknowledgments CT measurements at ENS Paris-Saclay have been financially supported by the French *Agence Nationale de la Recherche*, through the *Investissements d'avenir* program (ANR-10- EQPX-37 MATMECA Grant)

This work was performed using HPC resources from the *Mésocentre* computing center of CentraleSupélec and École Normale Supérieure Paris-Saclay supported by CNRS and Région Île-de-France (http://mesocentre.centralesupelec.fr/).

References

[1] W. Gao, Y. Zhang, D. Ramanujan, K. Ramani, Y. Chen, C.B. Williams, C.C. Wang, Y.C. Shin, S. Zhang, P.D. Zavattieri, 2015, The status, challenges, and future of additive manufacturing in engineering, *Comput. Aided Des.* **69,** 65–89

[2] Echeta, I., Feng, X., Dutton, B. et al., 2020, Review of defects in lattice structures manufactured by powder bed fusion. *Int J Adv Manuf Technol* **106**, 2649–2668

[3] H. Villarraga-Gómez, E.L. Herazo, S.T. Smith, 2019, X-ray computed tomography: from medical imaging to dimensional metrology, *Precis. Eng.* **60**, 544–569

[4] F. Borges de Oliveira, A. Stolfi, M. Bartscher, L. De Chiffre, U. Neuschaefer-Rube, 2016, Experimental investigation of surface determination process on multi-material components for dimensional computed tomography, *Case Stud. Nondestruct. Test. Eval.* **6**, 93–103

[5] M.-A. de Pastre, Y. Quinsat, C. Lartigue, Shape defect analysis from volumetric data - Application to lattice struts in additive manufacturing, 2022, *Precis. Eng.* **76**, 12–28.

[6] M.-A. de Pastre and Y. Quinsat, 2023, Virtual volume correlation of lattice structures: From volumetric data to geometrical and dimensional defects identification, *Additive Manufacturing*, vol. **61**, 103347

[7] S. Samper , F. Formosa, Form defects tolerancing by natural modes analysis, 2007, *J Comput Inf Sci Eng* 2007, **7**, 44–51

[8] D. Etievant, Y. Quinsat, F. Thiebaut, and F. Hild, 2020, A modal approach for shape defect measurement based on global stereo-correlation, *Optics and Lasers in Engineering*, vol. **128**, 106030

[9] Y. Qie and N. Anwer, 2022, Geometric deviation modeling for single surface tolerancing using laplace-beltrami operator, *Procedia CIRP*, vol. **114**, 19–24